Linearity of the Hamamatsu R11410 Photomultipler Tube at Cryogenic Temperatures for the LUX-ZEPLIN Experiment

Matthew Tan

Supervisor: Prof. Richard Gaitskell
Brown University, Department of Physics

A Bachelors Thesis submitted to Brown University
for the degree of Bachelor of Science in Astrophysics
May 8, 2018

Abstract

LUX-ZEPLIN (LZ) is an upcoming "Gen-2" direct dark matter detection experiment based on nuclear recoils in a two-phase liquid xenon time projection chamber. It is planned to be the most sensitive detector to date, and will check spin-independent WIMP nucleon cross sections down to 2×10^{-48} cm^2 at 50 GeV/c^2, covering a large space of the yet untested potential dark matter candidates. To detect the signals created by scattering events in the TPC, 448 3-inch diameter Hamamatsu R11410-20 Photomultiplier tubes have been commissioned for top and bottom arrays in the inner detector. These PMTs show a high quantum efficiency of $\sim$30% in the UV spectral range of xenon, have low levels of radioactive contamination, and are operable at liquid xenon temperatures. While photomultiplier tubes can be designed to exhibit good linearity for a wide range of incident light levels, the size of the S2 scintillation signal in LZ can potentially reach levels close to the non-linear range for the R11410. We test for the non-linear response of a R11410-10 PMT in the context of its relevance to LZ. In particular, the pulse linearity of anode output current and output charge at 5% deviation is determined at -100 $^\circ$C through illumination by pulses ranging from single photons to saturation size. In this thesis, two methods of accurately testing linearity in PMTs are described in detail as well as potential sources of design and measurement errors that must be addressed in order to achieve such a precise mapping of the PMT response. These methods have the advantage of only requiring two LEDs which do not need to be calibrated and thus can be repeated easily. The non-linearity of the PMT is discussed in-depth in the context of potential intrinsic and extrinsic factors. The signal gain of the photomultiplier tube is also studied at different voltages and compared with the theoretical response.

Contents

Chapter 1

Dark Matter

Over 80 years ago, dark matter was first suggested to exist by Jacobus Kapteyn based on stellar velocities. Since then, countless astronomical evidences have pointed towards the existence of cold non-baryonic dark matter [1]. This includes evidence from galactic rotation curves, large scale structure, gravitational lensing, and Cosmic Microwave Background (CMB) anisotropies. Unfortunately, the particle has remained elusive to direct terrestrial and indirect satellite means. With the most recent results of direct detection experiments LUX (Large Underground Xenon) and PandaX-II (Particle and Astrophysical Xenon Detector) failing to detect WIMP candidates, we now know that the WIMP cross section must be incredibly small if the mass is between 10 and 1000 GeV/c^2. The US Department of Energy and National Science Foundation have approved the construction of three new generation-2 detection experiments: LUX-ZEPLIN, which merges the LUX and ZEPLIN (ZonEd Proportional scintillation in Liquid Noble gases) groups will build a new 7-ton detector to probe masses above 10 GeV/c^2, while the SuperCDMS SNOLAB [6] experiment will probe masses below 10 GeV/c^2.

1.1 WIMPS

Astrophysical observations imply that 83% of the matter in the observable universe is dark, most likely of a non-baryonic nature. These observations include gravitational effects such as gravitational lensing, the rotational curve of spiral galaxies, and the velocity of the Bullet Cluster, as well as Cosmic Microwave Background data from anisotropies and acoustic peaks. Particle accelerators have been unable to produce

the elementary particles that would satisfy the requirements of dark matter, so new particle physics has been theorized to explain this missing component of our universe. In particular, supersymmetric extensions of the Standard Model predict the existence of a lightest supersymmetric particle (LSP) which is stable under R-parity conservation models and does not decay into any Standard Model particle. There have been many different particle candidates proposed as dark matter. A viable candidate must fit the properties of dark matter derived from astronomical observations: If dark matter was hot and had low mass, then it would have remained relativistic as structures began to form. This would subsequently "smear" out density fluctuations in the small scale early universe, which is inconsistent with the currently observed galactic structures in our universe. Thus cold dark matter candidates are favored.

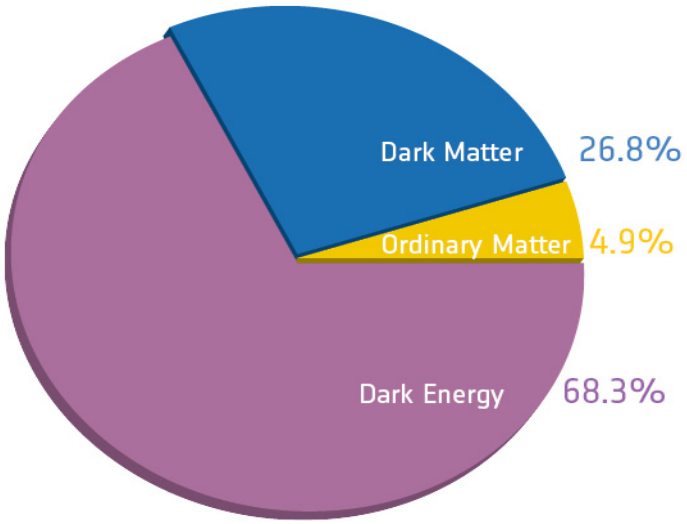

Figure 1.1: A mapping of gravitational leansing measurements from the Dark Energy Survey (DES) provides the most recent distribution of dark matter in the universe. This is consistent with the WMAP results. (Credit: ESA and the Planck Collaboration.)

The WMAP (2013) and Planck (2015) surveys of the CMB have reliably placed the percentage total mass-energy in a spatially-flat universe as 26.8% dark matter, 4.9% ordinary matter, and 68.3% dark energy, consistent with Type-1a supernovae surveys, and the strict predictions of Big Bang Nucleosynthesis from observed primordial light elements Deuterium and Helium-4 [2]. This is consistent with a Λ-cold (non-relativistic) dark matter model.

The most viable candidate is the Weakly Interacting Massive Particle (WIMP), which is the most promising modern candidate due to the 'WIMP Miracle'- WIMPs would be in thermal equilibrium with ordinary matter in the early Universe. As

the universe expands, the weak interactions of WIMPS would ensure that a relic abundance eventually "freezes out" due to negligible interaction rate, producing a density dependent upon annihilation cross section and the Hubble scale at freeze out temperature. For a WIMP of mass $\sim 10\ \mathrm{GeV}/c^2$ to a few TeV/c^2 and interaction close section 1 pb, this has been calculated to be remarkably close to the density determined from the astronomical observations.

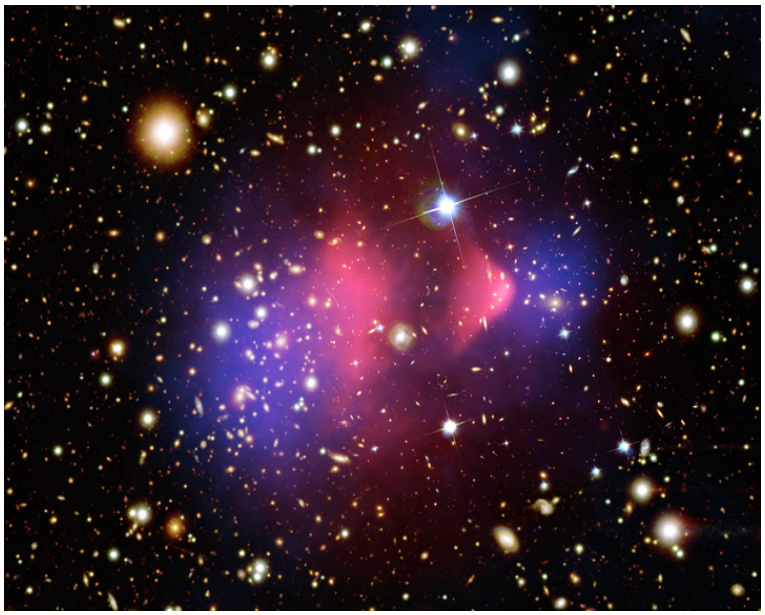

Figure 1.2: The Bullet Cluster currently provides the strongest evidence for dark matter particles due to its velocity distribution. (Credit: NASA/STScI; Magellan/U.Arizona/D.Clowe et al.)

1.2 Direct Detection

Direct Detection of dark matter is done in dedicated terrestrial experiments. As the Halo of the Milky Way passes through the earth, dark matter particles would scatter off target nuclei inside the detector and be discriminated from background signals. Usually these experiments are placed underground to shield from cosmic radiation such as muons. To discriminate the dark matter signal, methods involving energy deposition of phonons, scintillation light from photons, and ionization from electrons are used. These interactions take place in a fiducial volume which has the benefit of self shielding by the detector material.

Direct detection is dependent upon the local dark matter density distribution, which is estimated recently as $\rho = .22 \pm .07\ \mathrm{GeV\ cm}^{-3}$ (Bovy & Rix 2013), and the

local dark matter velocity distribution, which can be estimated as a normalized one-dimensional Maxwell-Boltzmann distribution dependent upon the velocity of the earth and velocity of the sun around the galactic center [3]. Past experiments have set large boundaries on the allowed spin-independent WIMP-nucleon scattering parameter space. As of 2018, the best exclusion bounds come from LUX, PandaX, and XENON1T (Xenon 1 ton). The US Department of Energy has approved the construction of two new experiments, LUX-ZEPLIN (Sanford South Dakota) and SuperCDMS at SNOLAB (Canada) to further constrain the parameter space of and hopefully detect the first WIMP signal.

Dark matter can also be detected through indirect means, as well as searches involving the LHC. Indirect detection involves the self-annihilation and decay products of dark matter such as neutrinos and antimatter, which then interact through multiple messengers and produce a detectable signal. For example, secondary electrons and positrons can produce radio synchrotron radiation. These cosmic and γ-rays can then be detected by telescopes. For particle accelerators, because dark matter particles do not interact electromagnetically and are non-baryonic, they tend to escape detection in colliders similar to neutrinos. This produces a quantifiable trace of missing energy which can then be detected.[4]

1.3 Liquid Xenon Noble Gas Detectors

Dual-phase time projection chambers (TPCs) using a massive dark matter target of liquid noble gas xenon are currently the most sensitive detectors searching for WIMP interactions. ZEPLIN-II, ZEPLIN-III, XENON10, XENON100, XENON1T, PandaX, and LUX are experiments using this principle, with the more massive LUX-ZEPLIN and XENONnT currently in construction.

Liquid xenon and argon have the benefits of being very low in background radiation, self-shielding, have the capability to localize the interaction vertex in three dimensions,and the ability to provide a simultaneous measurement of the scintillation and ionization signal from a particle interaction. This helps distinguish a potential signal from a background signal. A diagram of the working principle of a two-phase liquid-gas TPC is shown in figure 1.3. Xenon is preferred to argon in LZ for several reasons: removing impurities is easier and self-shielding is stronger. Also, the scintilla-

tion light of xenon is 178 nm, within the range of commercial photomultiplier tubes, while that of argon is 128 nm.

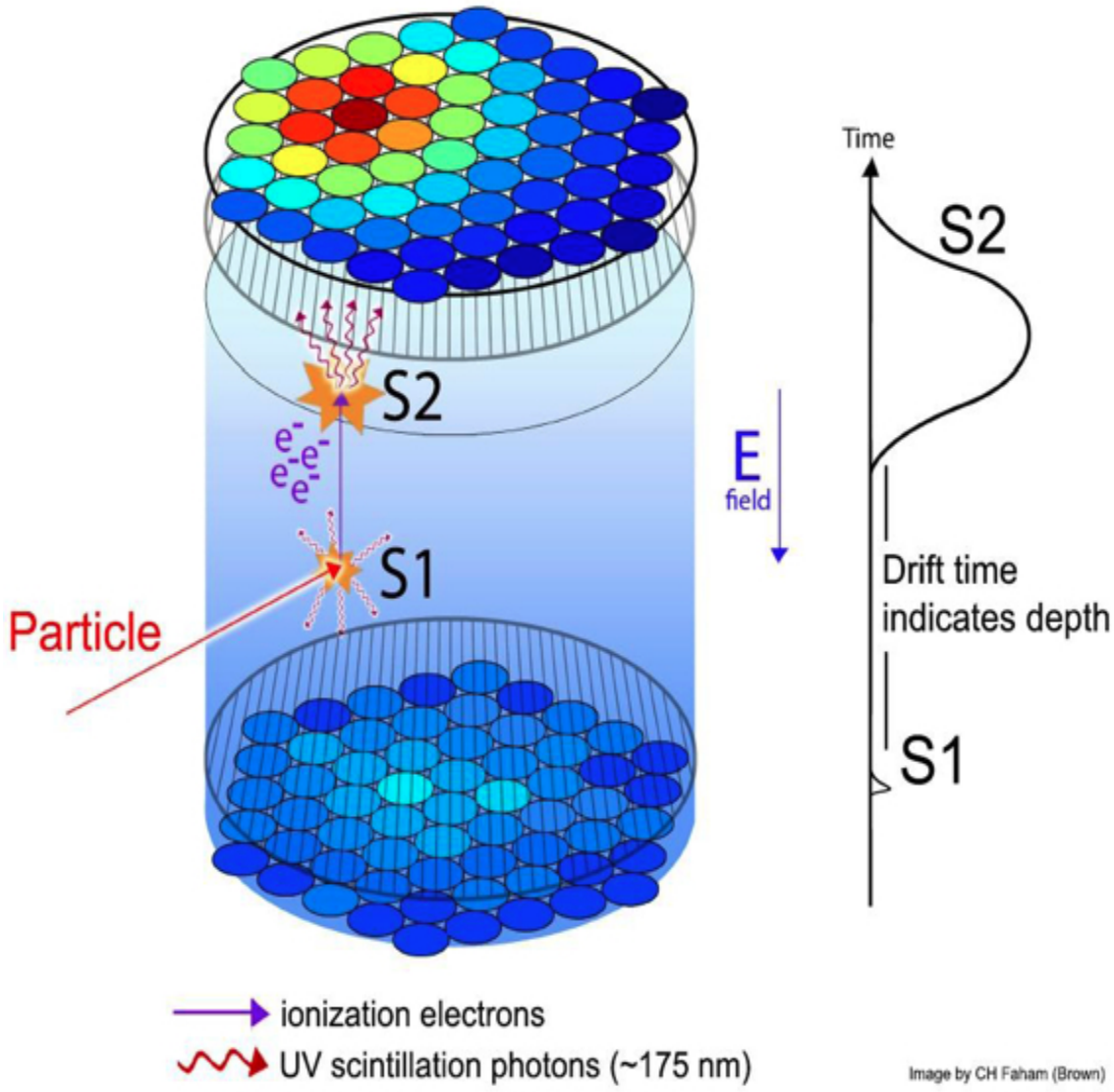

Figure 1.3: A scattering event will create an immediate primary scintillation signal (S1) and free electrons. These photons are detected by the photomultipliers. In the TPC, the electrons are drifted towards the gas by electric fields, and a large extraction electric field transports the electrons into the gas phase, creating the second scintillation signal (S2) through electroluminescence. The difference in time arrival of the signals measures spacial coordinate z as the velocity of electrons is constant. Coordinates x and y are determined from the S2 signal distribution relative to an array of PMTs.

1.4 LUX-ZEPLIN

LUX contained a 370 kg target LXe mass and ran from 2013-2016 in Sanford Underground Laboratory. 122 photomultiplier tubes were used to detect the 178 nm photons and electrons in the TPC. LUX saw no signs of WIMPs during its runs and has provided the most sensitive dark matter detection result during its operation, ruling out some of the theories on WIMPs.

LUX-ZEPLIN is an merger of the LUX and ZEPLIN dark matter detection experiments, to be located in the same Sanford Underground Research Facility (SURF). LZ began construction in August 2016 with approval of the US DOE, and is due for operation by April 2020. It has a projected 7 ton LXe mass active volume and a 3 ton LXe skin outer chamber and scintillator/water tank which serve as a muon veto. The projected sensitivity for spin-independent WIMP-nucleon cross sections will exclude values above 1.6×10^{48} cm^2 for a 40 GeV/c^2 mass WIMP [5]. To achieve this low sensitivity the photomultipliers must be able to discriminate the scintillation signal from both outside and PMT noise.

Like LUX, LZ is based off the xenon nuclei which recoil after being struck by oncoming WIMPS. The mass of the WIMP determines the kinematics of scattering, while the rate of scattering events depends on the exposure properties. The Hamamatsu R11410 photomultiplier tube has been designed specifically for using in a LXe TPC, and are placed in top and bottom arrays to view the active region. All photomultiplier tubes have eventually display non-linear output response with increasing light flux input and due to the potential size of the S2 scintillation signal reaching the non-linear region, the linearity of the R11410 must be calibrated.

1.4.1 PMT S2 signal in LZ

Electron recoil will be considered as it produces far greater yields than nuclear recoil. The yield of ionization electrons for electron recoils varies between 27 electrons/keV at low energies around 27 keV and 53 electrons/keV at high energies up to 2.5 MeV [6]. For a high energy 1 MeV event, NEST simulations show that an interaction in the liquid phase produces 30,000 electrons [15]. Assume that all the electrons are drawn up by the electric field and there is a nominal 95 % yield from liquid to gas phase. From the LZ technical report [6], most of the light from the S2 signal is

detected by the photomultiplier directly above it, and this photomultiplier has a *photon detection efficiency* of 10.2% [16], which includes the quantum efficiency of 30%, and the probability of a double emission is 22% (see section 2.6.2). This gives us an S2 pulse of around 4×10^6 photoelectrons. For a typical linear focused photomultiplier, onset of saturation occurs around 10 mA peak anode current, and the tube fully saturates (increasing light input does not increase the current any further) around 100 mA [7]. A S2 signal is around 1 μs in width, so the maximum currents correspond to a maximum charge of 6×10^{10} to 6×10^{11}electrons. For a PMT of gain 5×10^6 this is around 1×10^4 to 1×10^5 photoelectrons from beginning of nonlinearity to full saturation. Therefore, for a high energy electron recoil event, the S2 signal in the closest PMT in the top array will become saturated. In order to properly discriminate the size of the S2 pulse, it is critical to understand the linear response of the R11410 PMT.

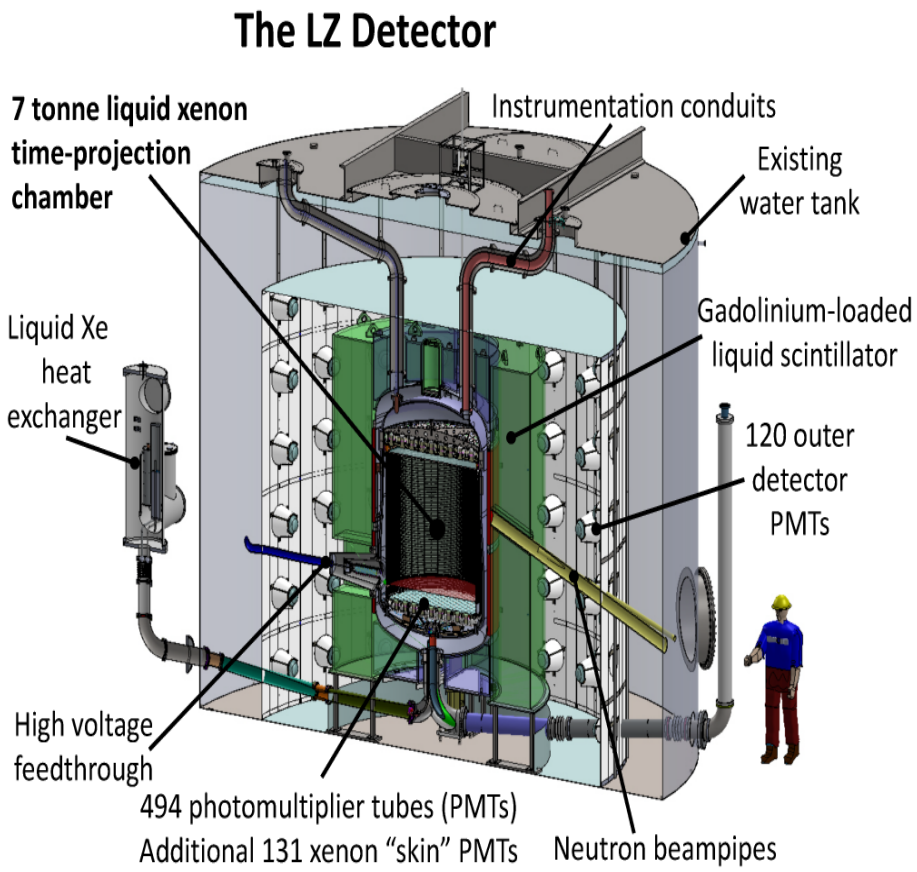

Figure 1.4: The LZ detector layout (Credit: LZ Collaboration.)

Chapter 2

Photomultiplier Tubes

In principle, the process of photoelectric photometry is simple: A photoemissive detector produces a current directly proportional to incident light intensity. Photomultipliers employ an electron multiplier system which allows detection even of single photons. In this way, photometry is dependent upon a simple electrical measurement with high accuracy. Unfortunately, the reality of photomultipler tubes is quite different from their "textbook" response. Many of the difficulties that plagued early photomultipliers 50 years ago are still relevant to modern tubes. In particular, their variation in gain with increasing light level is a significant problem for their use in experiments covering a large dynamic range of operation. While methods of design such as proper material selection, voltage-divider base usage, and dynode number and geometry can improve linearity, modern PMTs designed for high linear response still do not completely cover the upper range of potential S2 signals in LZ, as shown in section 1.4.1. Therefore, it is important to work through the steps in producing an accurate description of PMT linearity, which is explored in this thesis.

2.1 An Ideal Photomultiplier

An ideal photomultiplier tube works through two effects: the photoelectric effect and secondary emission. Light striking a photocathode in a vacuum tube will release photoelectrons, which are drawn towards a positively charged electrode called a dynode, where even more electrons are released due to the large initial electron energies. A typical gain at each dynode is 3 or 4, which with 10-14 dynode stages means that even a single photoelectron increases around 1 million times to become

detectable as a pulse at the anode. The probability of photoelectron emission is independent of light intensity so average current at the anode is directly proportional to light intensity.

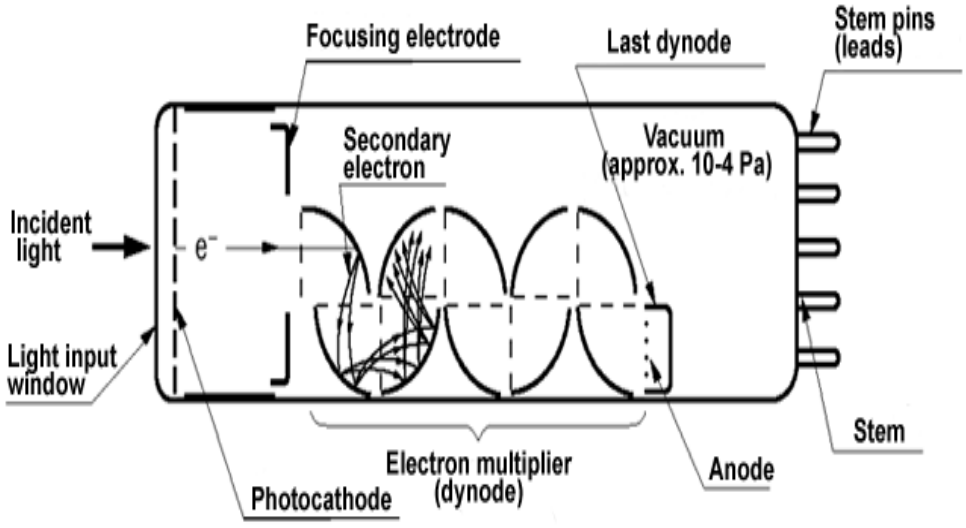

Figure 2.1: Internal components of a head-on Photomultiplier Tube (Credit: Hamamatsu Photonics.)

Unfortunately, in "real-life" photomultipliers are strongly affected by a multitude of different factors, including temperature, humidity, electric and magnetic fields, changes in operating potentials, and deviation from linear response. Interactions with associated hardware is complicated by the fact that a fix for one of the above-mentioned factors will often influence another. [9]

2.2 Photoelectric Effect

The Photoelectric effect (also known as photoemission), was discovered by Heinrich Hertz in 1887, and later explained by Albert Einstein in 1905-1906, using Planck's idea that matter absorbs radiation of wavelength λ only in quanta of energy

$$E = hc/\lambda \tag{2.1}$$

where Planck's constant is $h = 6.63 \times 10^{-34}$ m^{2}kg /s and speed of light is $c = 3 \times 10^8$ m/s.

Einstein proposed that electrons are bound to the material with energy W, known as the *work function*. Therefore, there is a lower limit of wavelength of light λ_c above which the photoelectric effect does not occur. To determine the work function, Energy of photoelectrons is zero at the threshold wavelength, so

$$\lambda_c = hc/W \tag{2.2}$$

For $\lambda < \lambda_c$, we have

$$E_{max} = hc/\lambda - W \tag{2.3}$$

This is the maximum kinetic energy that emitted electron may have; most will have less energy and many have insufficient energy to even escape.

Quantum Efficiency is defined as the probability of emission. In practice, the quantum yield per incident photon is used instead of quantum yield per absorbed photons. Photoemission is a linear process: the number of photons in a beam of monochromatic light is proportional to intensity, average number of photoelectrons emitted per second is proportional to intensity, and probability of photoemission remains constant.

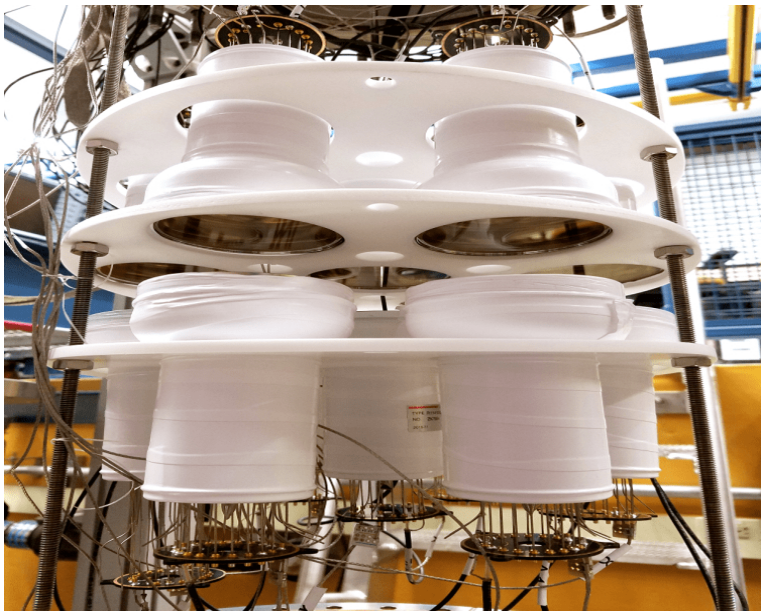

Figure 2.2: The Brown testing unit allows for 14 PMTs to be simultaneously tested in cryogenic temperature and pressure conditions (Credit: Brown University)

2.3 Secondary emission

The most sensitive electrometers require several hundred electrons to detect a signal. As such, the PMT utilizes secondary emission in each of its dynode stages to produce an easily detectable current. Pair-production provides the means for electrons to escape the dynode when an accelerated electron strikes it, similar to photoemission but with an energetic electron instead of a photon. The use of 10-14 dynode stages with a gain per stage of 3 to 4 will produce a gain of around 1 million, meaning that a photomultiplier can detect single photoelections.

2.4 PMT material selection

All of the Hamamatsu R11410 and R8778 PMTs to be used in LZ are each tested at Brown University in warm and cryogenic conditions. In the standard test, gain, single photoelectron (sphe) resolution, dark count, and other properties of PMTs are tested to meet the standards for operation in SURF. The Brown test chamber is shown in figure 2.2. This is done because PMTs are not all made exactly the same, and show variance over their different properties. It is helpful to understand the construction process that goes into producing a PMT, which explains the necessity of rigorous individual testing.

As described in section 2.1, a photomultiplier tube must have a window to allow photons to pass through, a photocathode for photoemission, a series of dynodes for secondary emission, and an evacuated envelope that allows for electrical connections.

In term of "real-world" PMTs, problems immediately begin to arise. Usually, the electrical connections must be metal, and thus have a large thermal expansion coefficient. This means the envelope must be made of a glass which can expand with a similar thermal coefficient. This "soft" glass is opaque to UV wavelengths, and so a window material of quartz or sapphire must be carefully sealed on. This provides a possible weak-point of mechanical integrity- for cryogenic applications such as in LXe detectors, care must be taken not to cool at an extreme rate lest the envelope detach from the window. This advice holds true even for PMTs specially made to handle extreme temperatures- Hamamatsu specifies one degree per minute for cooling to maintain long term health [8].

Another problem is that the materials used in photocathodes and dynodes have a high degree of chemical reactivity such as with oxygen and water vapor. Thus, a manufacturing problem arises as the cathode and possibly the dynode materials must be produced in the already evacuated and sealed envelope. Cesium and antimony (both used in the R11410 photocathode), have high vapor pressures and thus will evaporate and can deposit easily throughout the tube. Also, these two chemical elements decompose at temperatures of 80-200° C. Typically in vacuum tube construction, a "bake-out" is utilized- the object is heated to a very high temperature(600° C), in order to drive off volatile gases which can be absorbed by the materials. This lack of a high temperature bake-out process (they are still baked at a lower temperature) is the reason PMTs tend to exhibit after-pulsing.The chemicals used in the cathode and dynode stages also must not react with any of the other materials in the tube, or degrade each other. This tends to be a particular problem with alkali metals, which have one electron in their outer shell and are very reactive.

Obviously, a lot of precision and careful pre-selection of materials is required to produce a "healthy" photomultiplier tube. This is reflected in the high costs of a single tube (6000 USD) as well as the individual testing required of each of the 494 inner PMTs before they are ready for use in LZ.

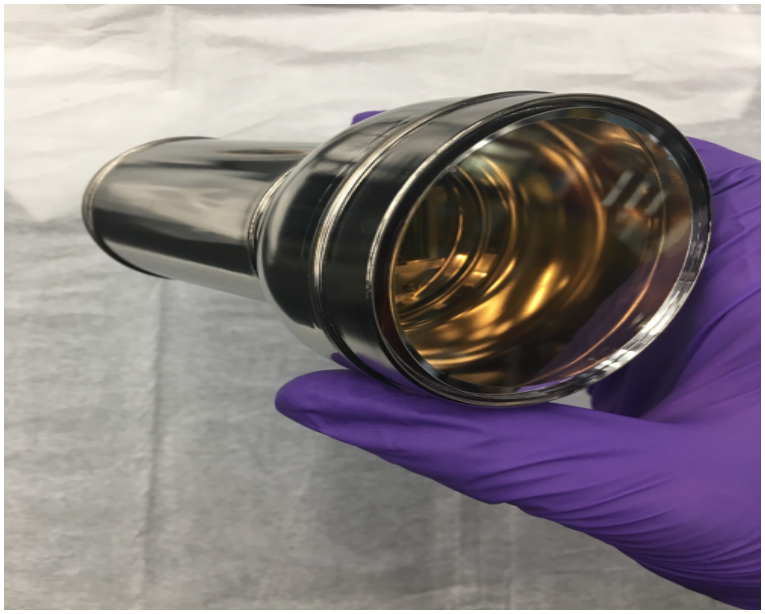

Figure 2.3: Example of an R11410-20 photomultiplier tube to be tested at Brown (shown head-on from an angle).

2.5 The 3-inch Hamamatsu R11410 PMT

The R11410 has been designed by Hamamatsu specifically for use in low temperatures down to -110 C. It is a head-on box and linear focused PMT and thus has a fast time response, good time resolution, and good pulse linearity. The photocathode is a biakali with a high quantum efficiency of 30%, and is single-photon sensitive to the scintillation wavelength spectrum of xenon. The window material is synthetic silica and is transparent to the 178 nm wavelength, transmitting UV radiation down to 160 nm. Synthetic silica, derived from quartz sand, is particularly susceptible to helium permeation so a nitrogen purge should be used for storage. A Kovar metal body provides excellent shielding from the earth's magnetic field due to a high permeativity constant.

There are 12 stainless steel dynode stages, and a typical electron multiplication factor g between 3 and 4 gives a gain around 5 million. A typical operating voltage is 1.5 kV with a maximum of 1.75 kV. It is operational at cryogenic temperatures and has very low intrinsic radiation because of careful materials selection, such as the use of a metal body instead of glass as well as ceramic electronic connections.

2.6 Gain

2.6.1 Voltage Dependence

Gain of a PMT is defined as the ratio of output current to input current. In terms of the anode current I_a and cathode current I_k,

$$G = I_a / I_k \tag{2.4}$$

Gain at each dynode g is proportional to the energy of incoming electrons, and can be represented as a power law of the voltage at each dynode.[8]

$$g = Av^p \tag{2.5}$$

for $p \leq 1$, decreasing with increasing voltage due to saturation effects. Note that g is the apparent gain at each dynode, and does not consider the secondary-emission yield. A detailed description of PMT gain would take into consideration the voltage

changes that occur as the electron avalanche propagates down the tube; however, a reasonable approximation can still be derived by assuming that individual current pulses produce a negligible change in interstage voltages.

The total tube voltage V for a tube with n identical stages is then

$$V = (n+1)v \tag{2.6}$$

Overall gain becomes

$$G = g^n = A^n[V/(n+1)]^{np} \tag{2.7}$$

We can find the value of p by taking the logarithm of both sides

$$\log_{10} G = n \log_{10} A + np(\log_{10} V - \log_{10} (n+1)) \tag{2.8}$$

It follows that

$$p = (1/n)(d \log_{10} G / d \log_{10} V) \tag{2.9}$$

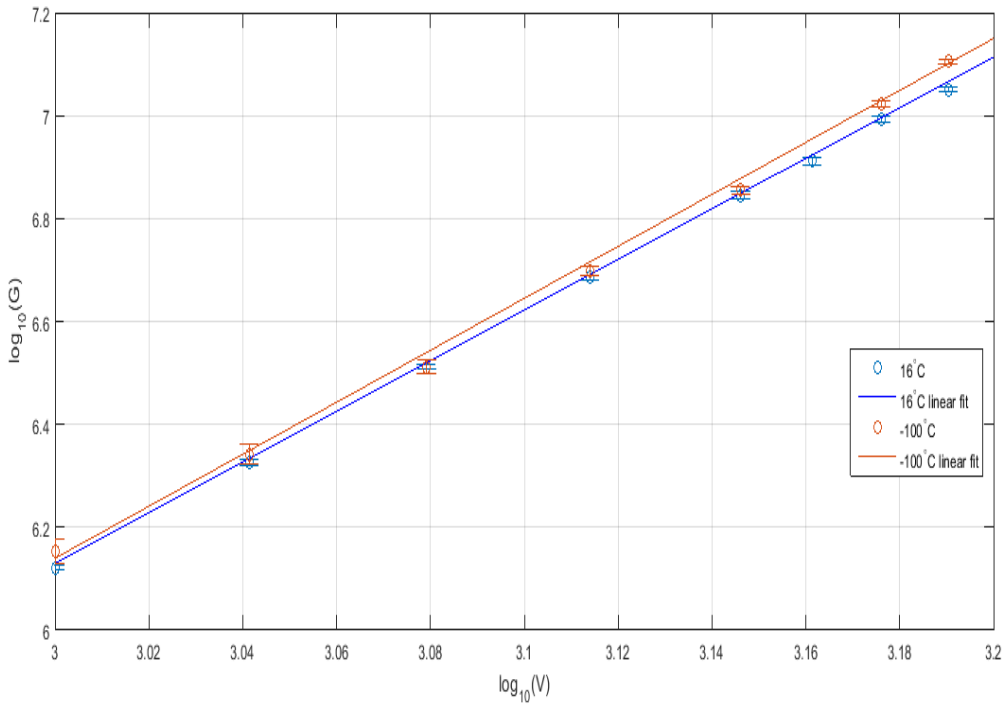

Figure 2.4: Relationship between input voltage and gain satisfies Eq.2.9. For our experiment we used a R11410-20 PMT, serial number KB0043.

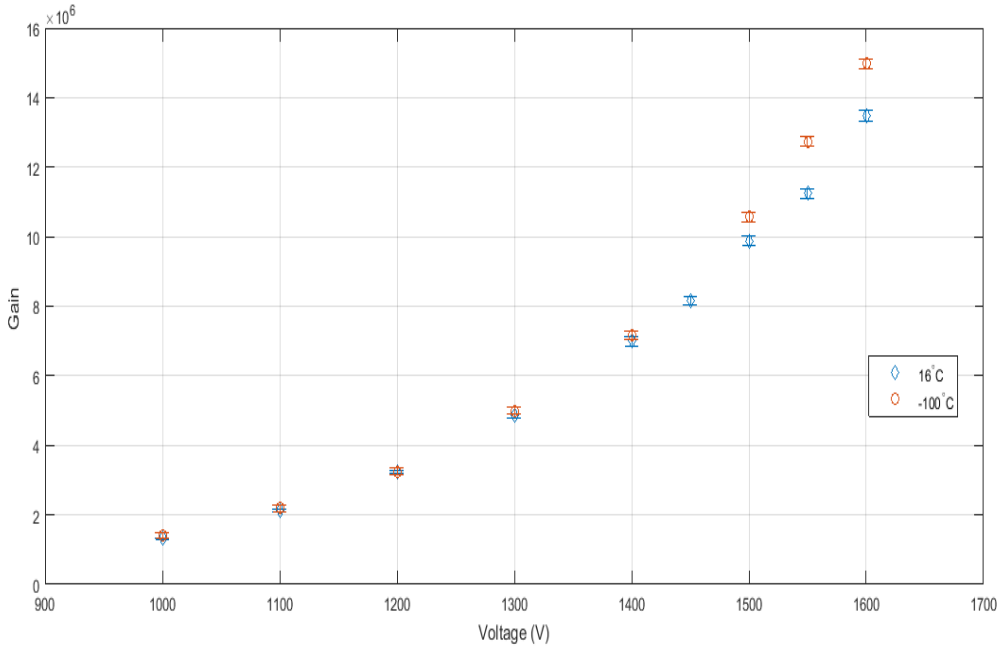

Figure 2.5: Relationship between input voltage and PMT gain. The R11410-20 PMT:KB0043 exhibits a high gain of $\sim 9.0 \times 10^6$ at 1500 V and room temperature.

The PMT used in our experiment was tested for gain vs. voltage from 1000 V to 1600 V. The R11410 model has n=12 dynode stages. A value of $np = 4.92 \pm .02$ at 16°C, and $np = 5.05 \pm .08$ at -100°C was calculated from the linear regression, shown in figure 2.4. This gives us a value of $p = .41 \pm .01$ and $p = .42 \pm .01$ for 16°C and -100°C respectively.

2.6.2 Dynode Stages and Poisson Statistics

Note that if we choose to differentiate Eq. 2.8 with respect to n, we have

$$d \log_{10} G/dn = \log_{10} g - np/(n+1) \tag{2.10}$$

For our PMT with $p \approx .5$ and $n = 12$, the constant term in Eq. 2.10 is .6, thus G increases as the number of stages increases if

$$g \geq .6e \tag{2.11}$$

So overall gain is highest if the number of dynodes are increased until Eq. 2.11 reaches the equality condition in order to maximize both gain and gain stability. For typical p values between .5 and 1, this means having an interstage gain of 2-3.

However, a higher gain per stage is usually chosen because of the statistical nature of the electron multiplier. The arrival of photons at a stage and its photoelectron emission can be approximated by a Poisson Process [7], by assuming that electrons are emitted at random with some probability. Therefore the probability of observing k photoelectrons for a given gain g,

$$P(k) = \frac{g^k e^g}{k!} \tag{2.12}$$

The probability of seeing no events $P(0) = .14$ for a gain of 2. As this is considered too many electrons to "lose", a gain of 4 to 3 is preferred [9], which produces a loss of around 2 to 5 percent respectively. Usually, this results in around 10-14 stages for a linear tube.

2.6.3 Experimental Determination of Gain

We can determine the gain of a PMT directly from the charge Q at the anode produced by a single photoelectron. Single Photoelectrons (sphes) can be produced easily by pulsing a LED of sufficiently low light level, such that P(2) from Eq. 2.12 becomes negligibly small. The light level should be changed at this level and the peak of the Gaussian distribution of charges should not change, only number of counts. Gain is given by

$$G = \frac{Q}{R_{\text{eff}} * q_{\text{e}}} \tag{2.13}$$

Where $R_{\text{eff}} = 25\ \Omega$ is the effective resistance of the PMT base in parallel with the DAQ or amplifier input resistance and $q_e = 1.602 \times 10^{-19}$C is the charge of an electron.

2.6.4 Stability

If we take the logarithm of Eq. 2.9 then we have the stability of photomultiplier gain as a function of voltage:

$$dG/G = np(dV/V) \tag{2.14}$$

For a typical tube with $np \approx 10$, the stability of the voltage source must be a magnitude greater than desired gain stability. The CAEN Mod N470 High Voltage Power supply used in our experiment has a long term voltage stability of ± 2 V. At the standard 1500 V bias voltage this means we can get 1% stability in gain as a result of our power source.

As the goal of this thesis is to determine the 5% deviation from linearity of our PMT, we can see that problems have already begun to arise that might influence our experiment. The other possible sources of error and techniques for minimizing these sources are addressed in the next chapter.

Chapter 3

Experimental Set-Up

This chapter describes the test apparatus used to test a single PMT, as well as the method of cooling, electronics, and data collection.

3.1 Apparatus

As shown in figure 3.1, the single photomultiplier tube is suspended facing upwards in the sealed chamber and configured such that the anode is grounded. This mimics the set-up in LZ where it is used in order to minimize a distortion when connecting with an amplifier or readout electronics[6] . Feedthroughs connecting the signal and high voltage connectors are located at the top of the chamber. This includes a signal output to the oscilloscope and from the LEDs to the pulse generator. Inside the chamber is a 430 nm blue LED (LED 2 in figure 3.1) incident upon the middle of the PMT, and an optical fiber connected to another 430 nm LED located outside the chamber (LED 1 in figure 3.1).

A CAEN Mod N470 High Voltage power supply was used to bias the PMT. A Tectronix AFG 3102 function generator supplied fast pulses to each LED through separate channels, and the PMT output signal was digitized by a Picoscope digital oscilloscope with a 1 GHz sampling rate.

3.2 Cooling Method and Gas System

A Pfeiffer vacuum system shown in figure 3.1 is first used to evacuate the chamber to around 1×10^{-4} bar. Then nitrogen gas is added to the chamber. This is because the freezing point of water vapor in air is 0°C and ice particles can damage the photocathode as described in Chapter 2.

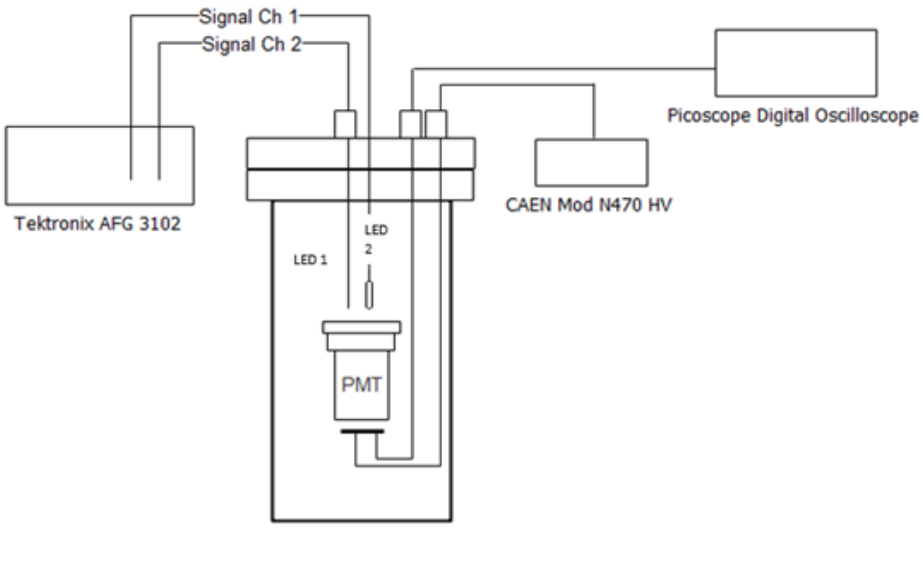

Figure 3.1: Schematic of set-up used for measurements of sphe and linearity.

A pure ethanol bath as shown in figure 3.2 was placed around the chamber such that the photomultiplier is encompassed. Liquid nitrogen is added to cool the ethanol until it had a jelly-like consistency, as its freezing point is -115°C. The chamber is then slowly cooled from room temperature 16°C to -100°C over the period of 2 hours. Large temperature gradients should be avoided in order to minimize cesium migration.

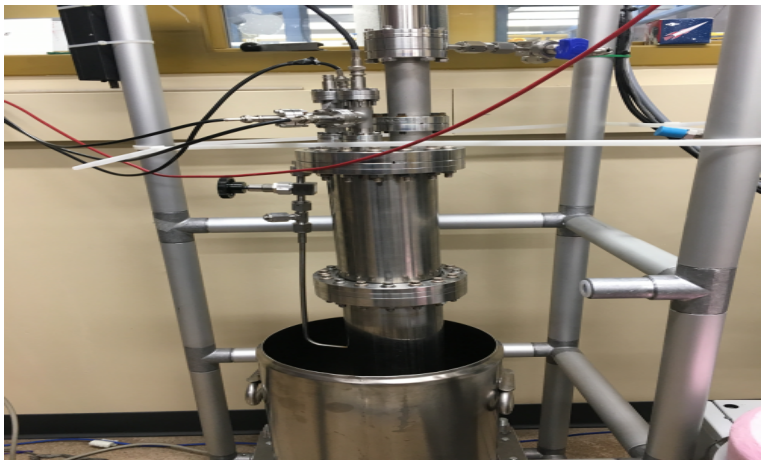

Figure 3.2: PMT chamber cooling process

Thermal conductances in typical PMTs are on the order of 1 mW/°C, and thermal transfer in a tube depends mainly on radiation instead of conduction. Therefore, after cooling to -100°C, the photomultiplier tube should be left for around 1 hour before taking data to become stable [8]. Gain was also measured around every 20 degrees, and it was found that gain increases by .15%/°C for cooling.

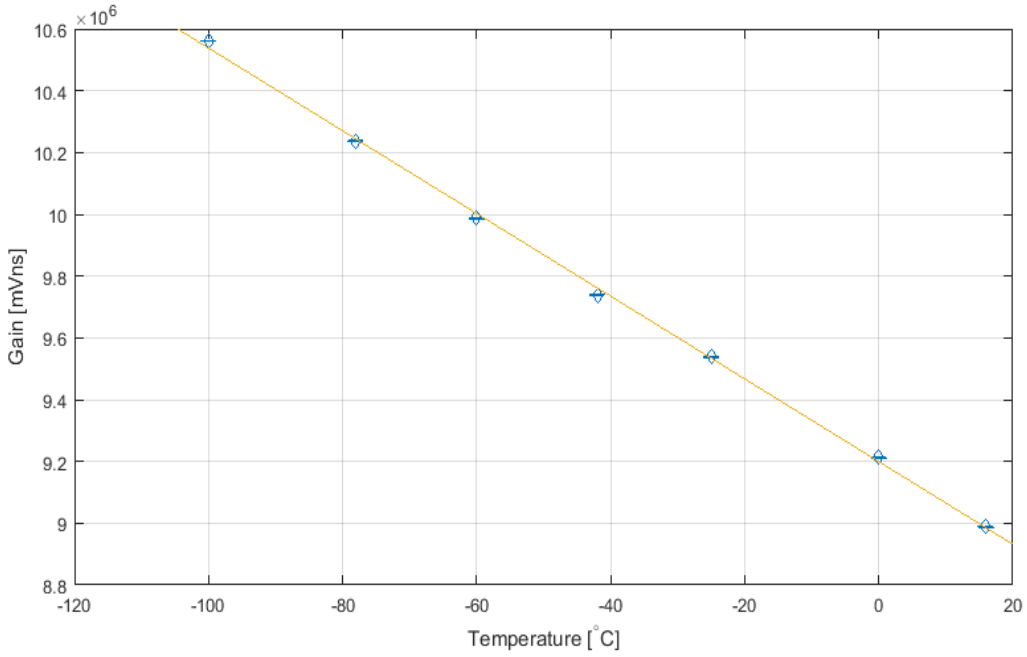

Figure 3.3: Gain was measured periodically during the cooling process at an input voltage of 1500 V. PMT: model R11410-20, KB0043

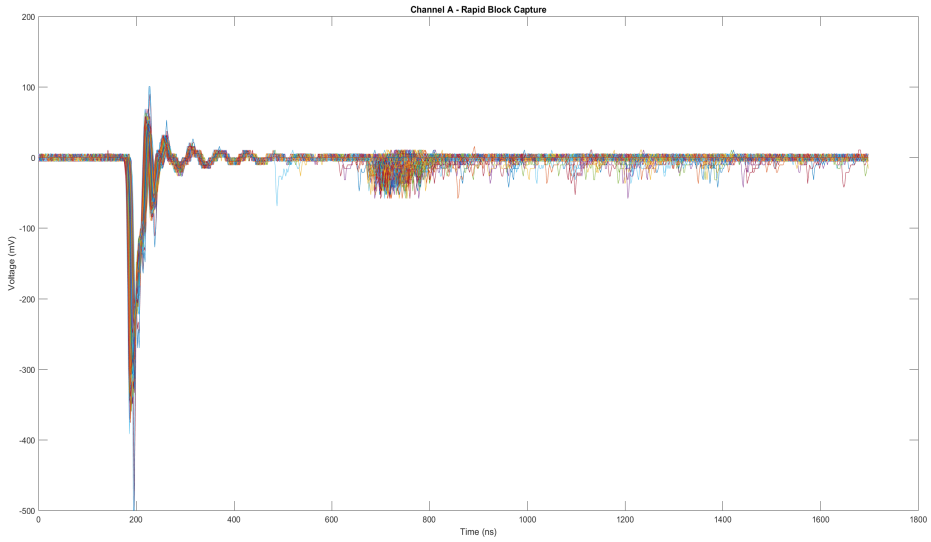

Figure 3.4: The Picoscope main data taking code digitizes 10,000 pulses set with a specific trigger. These pulses can then be integrated to produce a charge spectrum. Picoscope is programmed to record 550 events after the initial trigger event, at a sampling period of 2 ns.

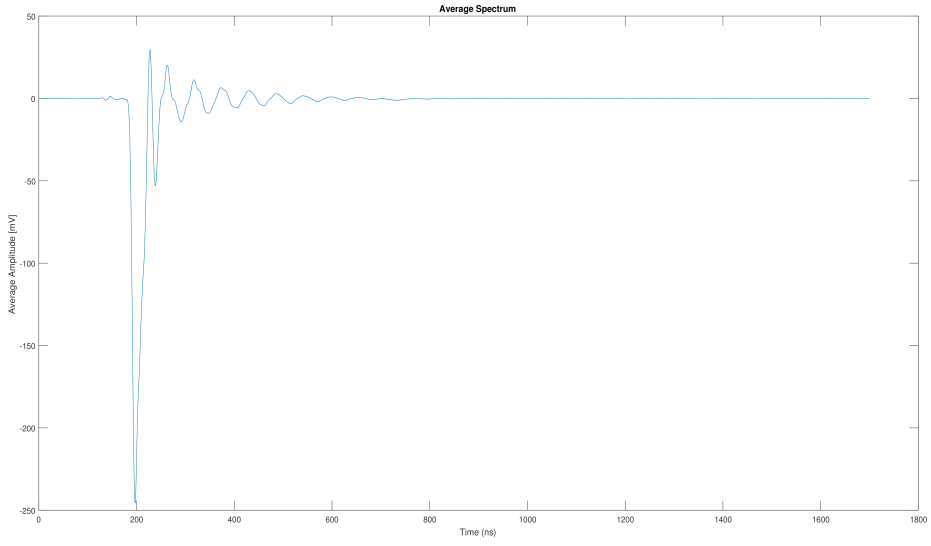

Figure 3.5: The average of the 10,000 pulses for visual reference. In this example, input square pulses to the LED were 20 ns in duration.

3.3 Gain Measurement

If the PMT is illuminated with single photoelectrons, it will produce an output signal at the anode with a spread in charge about the mean. We adjust an incident light to low enough level such that primarily single photoelectrons are produced, and set the threshold on data acquisition through Picoscope software to eliminate the pedestal noise events. The charge of each event is calculated from the integral of the pulse. 10,000 events captured are used to create the sphe spectrum which follows a Gaussian, as shown in figure 3.6.

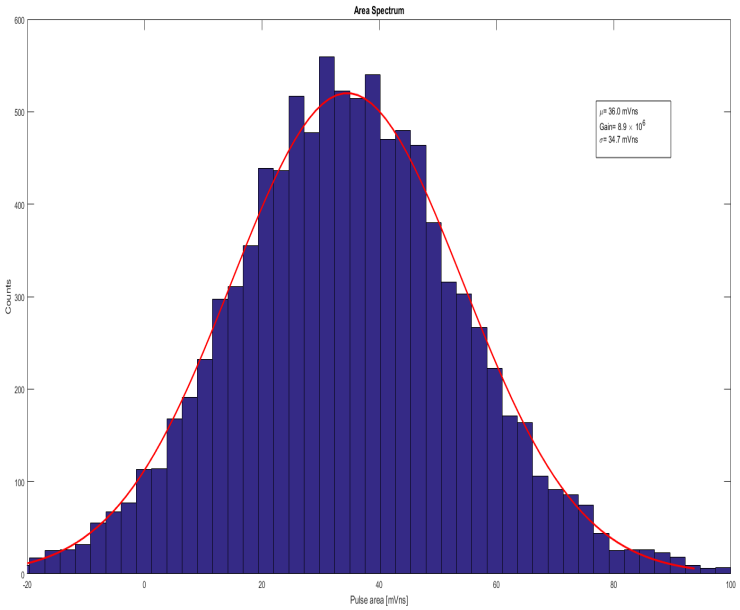

Figure 3.6: Schematic of set-up used for measurements of sphe and linearity. In this example, the mean area is 36.0 mVns, corresponding to a gain of 8.9×10^6. The Gaussian fit has standard deviation 34.7 mVns. PMT: model R11410-20, KB0043

3.4 Linearity Measurement

Non-linearity was determined by measuring the change in amplitude of the combined response when a small constant input pulse to the LED transmitted by an optical fiber is incident with a variable input pulse of the other LED. The optical fiber was used for the small pulse in order to provide better stability by directing light directly to the center of the PMT. If the variable pulse produces an anode current of I, the constant small pulse I_s, and the combined pulses produce an anode current of $I + \delta I$, then

comparison between δI and I_s leads to an integral non-linearity measurement. For our experiment we used pulses of width 100 ns and frequency 1kHz.

3.5 Gain Stability

Photomultipliers exhibit both short term and long term gain shift. Short term gain shift is called drift, taking place over the period of minutes to hours. It is greatly reduced through longer operating time. [8] As such, Hamamatsu recommends warming-up the PMT for 1 hour to minimize short term shift. It is also recommended to take the linearity measurement as fast as possible [7]. We warmed up our R11410 PMT for 1 hour and measured the drift of a 1 μA mean anode current every 10 minutes for a 4-hour period- stability was within 1% over this period.

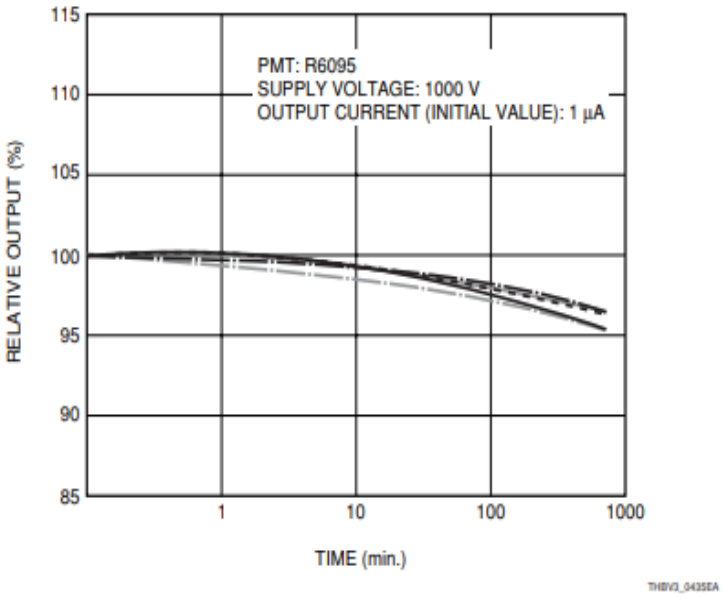

Figure 4-35: Examples of drift data

Figure 3.7: Credit: Hamamatsu [8]

Chapter 4

Linearity

There is no universally agreed upon definition of linearity for a photomultiplier tube, and many different methods of measurement have been described [8]. We will define it as the ratio between an input light flux and its corresponding signal output. For the purpose of direct dark matter experiments, with respect to the S1 and S2 scintillation signal, our focus is on pulsed charge linearity, as we are concerned with number of photons incident on the PMT from single electroluminescence events. As was shown in chapter 3, attempting to probe low single percentage deviations from linearity is particularly sensitive to systematics so care must be taken in the experimental method. Hamamatsu places the pulsed 5% nonlinearity measurement for the R11410 at 20 mA.

4.1 Method of Measurement

We could try to merely flash an LED incident on the PMT window with increasing rectangular-pulse voltage heights in order to get a curve of PMT response as a function of light flux. However, LEDs exhibit their own response curves and gain drift. The natural solution that does not require calibrating the LEDs, is as follows: two independently triggered LEDS with their own power supply are each placed incident on the PMT face. Care should be taken to minimize crosstalk between the LEDs to under 1% - this may be tested by completely obscuring one LED with clay while feeding pulses into the other, and then both LEDs. They are set so that the output peak anode current is the same, which can be done using the oscilloscope. When they are switched on the same time, the combined peak current should be the sum of the individual peak currents if the PMT is in the linear region, and should deviate from that value when

the PMT begins to show non-linear effects, similarly for the charge. This is shown in figure 4.1.

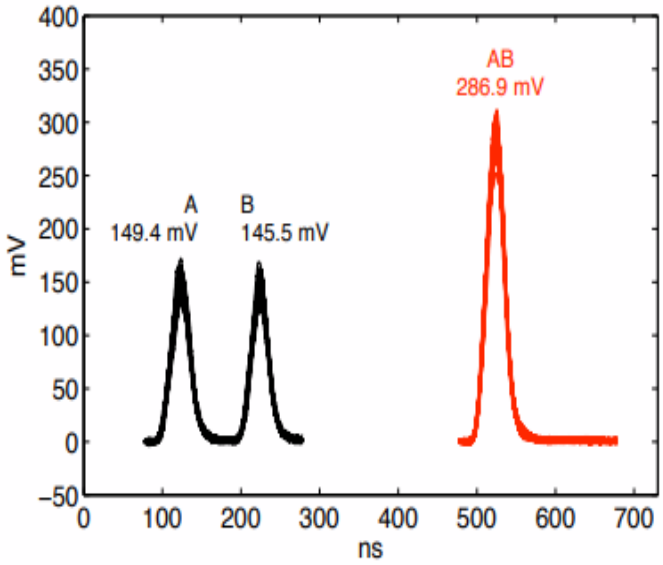

Figure 4.1: Example: The pulse generator sends 100 ns pulses to the LED which produces the response with height $I(\phi_1)$ and $I(\phi_2)$ in sequence. Then the pulses are set at the same time and we get $I(\phi 1 + \phi 2)$. The same can be done for charge by integrating each pulse. (Credit: Carlos Faham)

Unfortunately, this method runs into an obvious problem: nonlinearity can be measured for very low percentages accurately but as the percentages get higher, it underestimates the true value as the individual pulses will exhibit their own non linear effect. Two improved methods are described in the next sections.

If we have two independent light sources ϕ_1 and ϕ_2, then linearity is defined as

$$I(\phi_1 + \phi_2) = I(\phi_1) + I(\phi_2) \tag{4.1}$$

While a PMT is output is non-linear if this equality is not upheld. Integral non-linearity is defined as:

$$\Delta I / I = \Delta G / G \tag{4.2}$$

4.1.1 Step Method

This is a step method which corrects for the underestimate of the magnitude of non-linearity that arises from adding two pulses of equal size, by placing the input flux ϕ at the correct location. We start with two LEDs each set such that I_ϕ is say for example 10mA. Then, $I(\phi_1 + \phi_2)$ is confirmed to be 20mA so this point is plotted with 0% deviation from linearity. Now say that the two LEDs are each set to 20mA and the output current is 38mA.The nonlinearity of $2/40$ is plotted with the point 38mA. The two LEDs are now set to 38mA and the output current is 74mA. The nonlinearity of $6/80$ is now associated with the point 76mA, and so on. The method is then repeated with a different starting point. One problem is this method is that data taking is slow because the function generator must be adjusted to provide the correct pulse size for every data point, whereas data should be taken as quickly as possible to minimize gain shift (section 3.5). Another problem is that any systematic errors in the set-up accumulate over the measurements. Typically we might need 5 measurements to probe the non-linear response. If we even have a 2% systematic error, then we can potentially get a 32% error for our last measurement.

4.1.2 Large Variable and Small Constant LED Measurement

In this method, one LED is kept at a small constant level while the other is set to a variable height. This is the method proposed by [10] for precise linearity measurements. The onset of integral non-linearity can be determined by noting the difference between the fixed value of the small pulse and the variable and small pulse combined. This method also eliminated the problems described above, and has the benefit of being less sensitive to systematic errors. For our experiment we chose the size of the small pulse to have a 100 mV height, knowing that according to the manufacturer nonlinear effects would occur around 500 mV. Frequency remained constant at 1 kHz throughout the measurement and pulse size constant at 100 ns fed into each LED. It was confirmed that the combined pulse was also 100 ns in width.

4.2 Theory

4.2.1 Anode Current vs. Charge

While PMT pulses are not completely symmetrical in terms of shape, if we assume linear operation then peak pulse height should be proportional to total charge at the anode. However, non-linear effects are also associated with mean anode current. [9] To change from mean anode current to peak anode current we can multiply the peak value by the pulse width of 100 ns and frequency 1000 Hz. So for a 10 mA peak anode current it is roughly 1 μA mean current.

Therefore, we must ensure that all measurements are taken at the same rate of 1 kHz and that the mean anode current remains relatively low; A value $\leq 1\mu$A over the duration of our measurement is recommended by [7] and [9]. As shown in Figure 2, we tested the PMT output peak current vs. charge in the range where we are probing, as well as over a large dynamic range, up to the point where the peak current stops increasing with increasing incident light (full saturation). The linear relationship is apparent for the range relevant to our interest ($\sim 1 - 25$ mA peak current), while deviations occur for higher currents. The reason that current and charge pulsed nonlinearity eventually deviate is theorized to be because space charge saturation is strictly dependent upon the instantaneous current, (section 4.2.4) and not the charge [7].

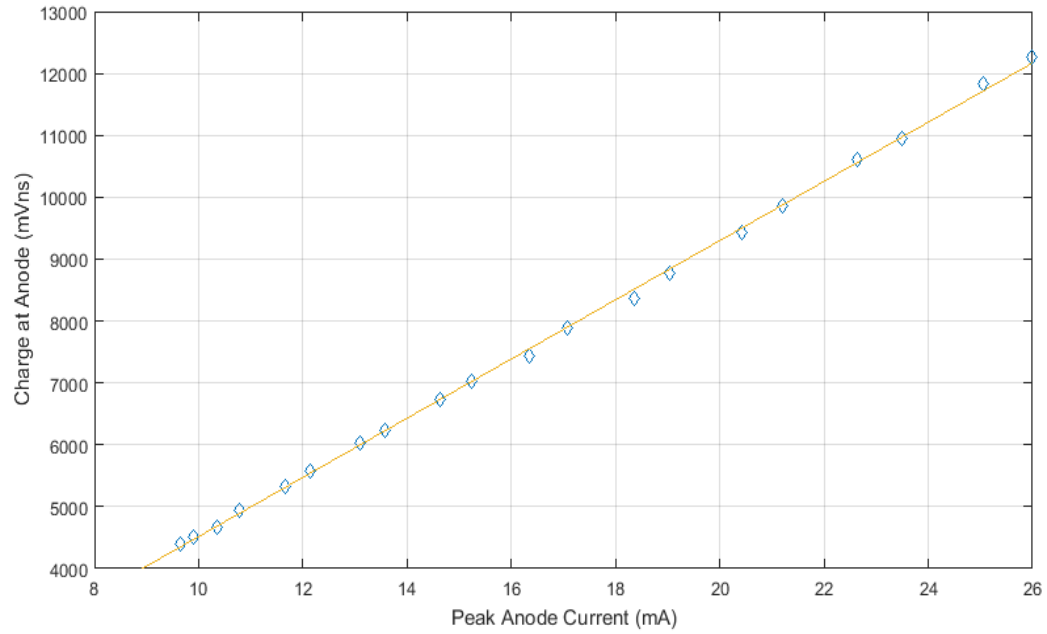

Figure 4.2: The relationship between peak anode current and charge is linear for low values of current. This range covers the projected location of 5% deviation from nonlinearity as specified by Hamamatsu.

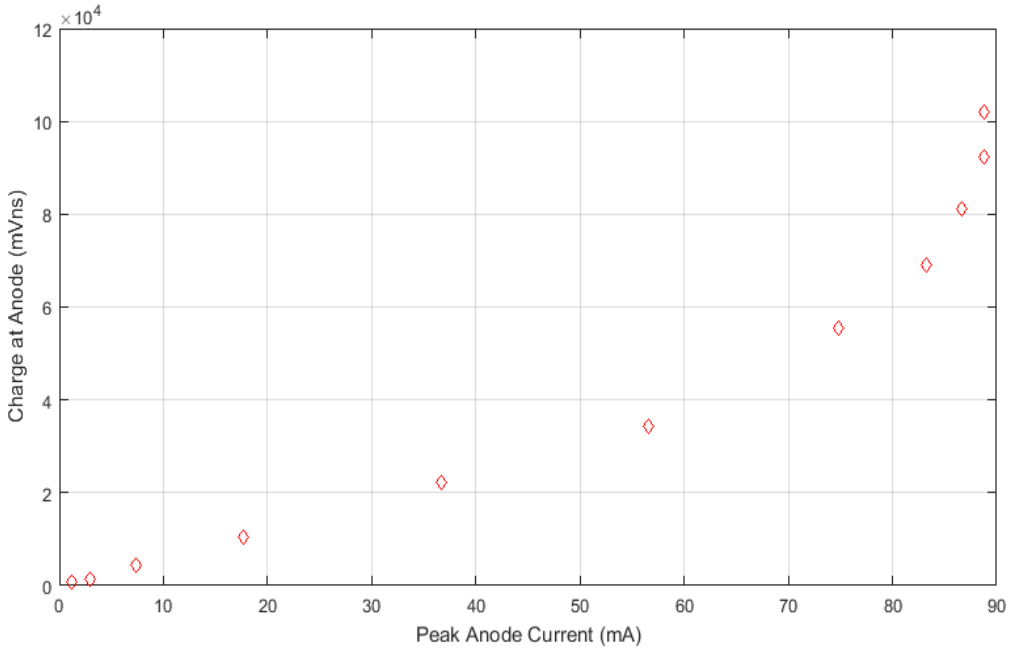

Figure 4.3: If we increase the incident light further we can see that the peak anode current saturates at about 88 mA while the pulse shape gets wider and thus charge continues to increase.

4.2.2 Voltage-Divider

When a PMT is operated, a series of voltages must be provided to each dynode stage to accelerate the electrons towards each subsequent stage. This is achieved through a single supply using a resistive divider network. The potential difference between the photocathode, dynodes and anode are regulated in order for optimal linear performance, signal-to-noise ratio, and power dissipation. The circuit diagram shown in figure 4.3 is for the Hamamatsu R11410 PMT. It is a tapered divider, which employs higher resister values near the photocathode to improve signal-to-noise ratio, and higher values near the anode to minimize space charge effects [11]. A readily apparent source of non-linearity is then determined from the circuit itself- drawing an anode current will produce a voltage drop across the last resistor that influence the voltages of the previous resistors, affecting the interstage gain.

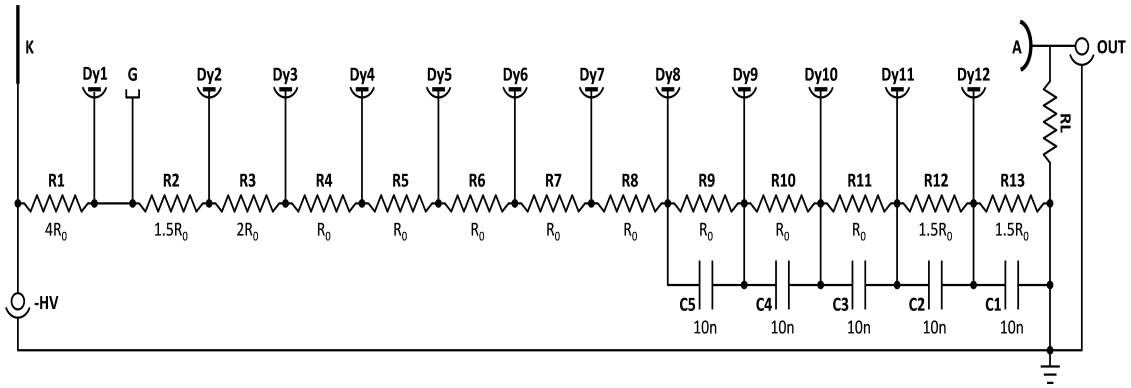

Figure 4.4: The R11410 tapered voltage-divider circuit with 5 reserve capacitors. $R_0 = 5\text{M}\Omega$ and load resistance $R_L = 50\Omega$. Note that our output electronics have an input impedance of 50Ω in parallel with the load resistor, so the effective resistance used for converting between anode voltage and current is 25Ω. [12]

For a rough estimate of this effect, suppose that gain is very high such that only the last dynode stage has a relevant current, which is the anode current minus the negligible current from the previous dynode. Also assume that all the resistors have the same resistance R. The anode current decreases the voltage across the last resistor by $I_A R$. The anode collection voltage then drops by that same amount and the voltage across all dynodes increases by the same amount. This is equivalent of increasing the overall voltage by

$$dV = I_a R(n+1)/n \tag{4.3}$$

It follows that

$$dV/V = I_a R/V\dot{(}n+1)/n = (1/n)\dot{I}_a/(I_D + I_a). \tag{4.4}$$

Using Eq. 2.14, we have

$$\Delta G/G = np(dV/V) = p(I_a/(I_D + I_a)) \tag{4.5}$$

If we neglect tube currents, then $I_D + I_a$ is a constant $V/(n+1)R$. This change in gain manifests in an over-linearity as anode current increases [9].

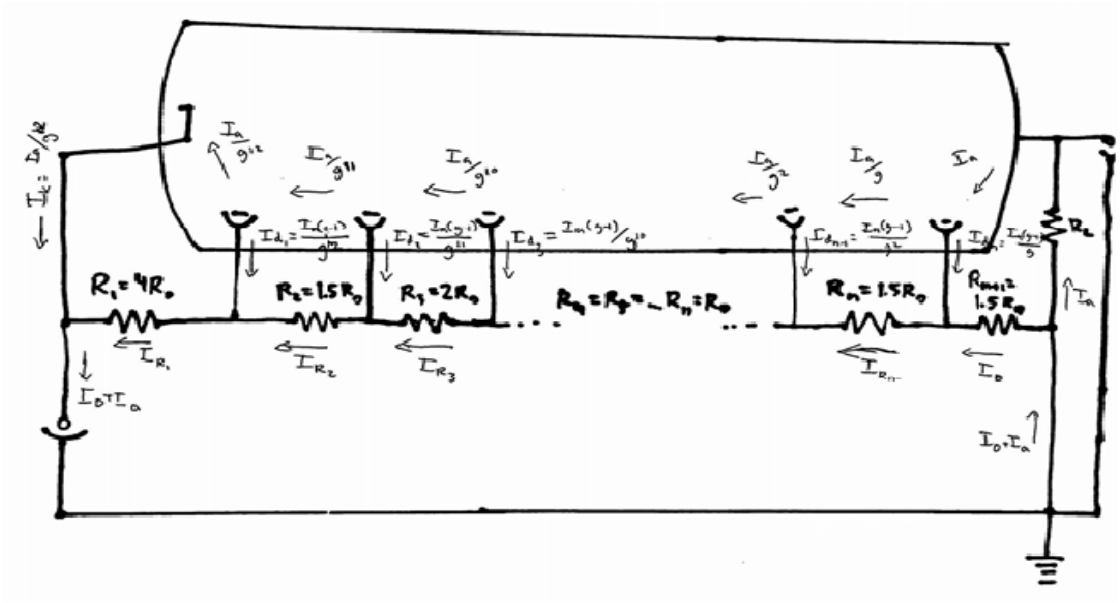

Figure 4.5: Circuit Diagram for the R11410 PMT and base. Currents shown are conventional. There are n=12 stages and $R_0 = 5\text{M}\Omega$

We can also do a more detailed analysis in order to get a better estimate of where this effect will occur at the 5% level with respect to our PMT. Consider the circuit diagram in figure 4.5 which shows the resistor currents, tube currents, and currents from the dynode multiplication chain derived from Kirchoff's rules. As before, current through the divider when there is no anode current is

$$I_{D0} := (V_{HV})/(R_{total}) = V/(n+1)R \tag{4.6}$$

With an anode current drawn we solve the circuit and find for our 12 stage and interstage gain $g = 3.8$ PMT, the current across the last three resistors decreases while

the rest increase.

$$\begin{aligned} I_{R1} =& I_{D0} + I_a \frac{g}{(n+1)(g-1)} - \frac{I_a}{g^n} \\ I_{R2} =& I_{D0} + I_a \frac{g}{(n+1)(g-1)} - \frac{I_a}{g^{n-1}} \\ & \dots \\ I_{RN} =& I_{D0} + I_a \frac{g}{(n+1)(g-1)} - \frac{I_a}{g} \\ I_D =& I_{D0} + I_a \frac{g}{(n+1)(g-1)} - I_a \end{aligned} \tag{4.7}$$

The net increase in gain can then be derived, first by computing the interstage change in gain for each current I_{Ri}:

$$\frac{\Delta g}{g} = p\frac{dI_{Ri}}{I_{Ri}} = p\frac{I_{D0} - I_{Ri}}{I_{D0}} \tag{4.8}$$

The overall change in gain is computed as the summation and we obtain the final result:

$$\frac{\Delta G}{G} = \frac{I_a}{I_{D0}}(1 - \frac{g}{(n+1)(g-1)}) \tag{4.9}$$

This is the same result stated in [14]. For our R11410 PMT, we have an interstage gain of $g = 4$. The overall resistance of the circuit is 92.4 MΩ, and at a bias voltage of 1500 V we have $I_{D0} = 16.2\mu$A. This translates to a 5% over-linearity at around 1μA mean anode current, or at 1 mA peak anode current for width 100 ns pulses at 1 kHz.

4.2.3 Reserve Capacitors

To eliminate this source of non-linearity in pulsed applications, reserve capacitors (commonly referred to as *decoupling capacitors*) have been carefully designed and implemented into the LZ bases. These provide a reserve charge which prevents the changes in interstage voltage described by Eq. 4.7. If we have an average charge of an anode pulse as xGq_e, for x photoelectrons at the cathode and q_e the charge of an

electron, then the capacitor of the last resister must resist a voltage change of

$$dV = -\frac{xGq_e}{C} \tag{4.10}$$

From Eq. 2.14, substituting Eq. 4.19, and rearranging, we have

$$C > \frac{npxGq_e}{V(dG/G)} \tag{4.11}$$

For a high energy 1 MeV event producing an S2 signal of 4×10^6 photoelectrons (section 1.4.1), at a bias voltage 1500 V and with p=.5 (section 2.6.1), the 10 nF decoupling capacitor commissioned for LZ will provide maximum 120% gain change per pulse. Thus the capacitance of 10 nF is not sufficient to resist the voltage change from a high energy electron-recoil event. For an event of 1×10^4 photoelectrons which corresponds to peak anode current of around 10 mA for 100 ns width and 1 kHZ frequency, the gain change is 0.3%. Note that we are only considering the last reserve capacitor nearest the anode as the charge is decreased by a factor of $g = 4$ as we move down the resistor chain.

We can also use Eq. 4.11 to confirm that the RC time constant of the voltage-divider is small compared to the frequency of pulses f.

$$R < 1/fC < \frac{V(dG/G)}{fnpxGq_e} \tag{4.12}$$

For our final resister $R_D = 7.5$ MΩ, and pulses with frequency $f = 1000$ Hz, if we want a maximum gain change of 1% then the capacitors will recharge for events up to 400 photoelectrons.

4.2.4 Space Charge

If we use an LED to gradually increase the incident light on a photomultiplier until the output peak current goes past $\sim$100 mA (For a linear-focused PMT), we can visually see the PMT signal begin to saturate- the height stops increasing in linear steps, the peak begins to flatten, and the tail extends further. This type of non-linearity in pulsed applications is due to space charge saturation at the last few dynode stages.

[7] This effect causes the trajectories of some electrons to change, and some electrons get reflected back to the dynode from whence they came, decreasing the gain. Space charge can be modeled by the Child-Langmuir equation, which gives the maximum space-charge-limited current in a planar diode with infinite radius [13]. We start with Poisson's equation

$$\nabla^2 V = -\rho/\epsilon_0 \tag{4.13}$$

For voltage V between dynode stages, and $\rho = J/v$ for current density J and velocity v. Relating kinetic energy of an electron to its electric potential energy, we also have

$$(1/2)mv^2 = -qV. \tag{4.14}$$

It follows that

$$\nabla^2 V = J\epsilon_0^{-1}\sqrt{m/(2q)}V^{-1/2} \tag{4.15a}$$

$$= kV^{-1/2} \tag{4.15b}$$

For a constant k. Then we can solve this differential equation to get the desired three-halves power law.

$$J = \frac{4\epsilon_0}{9}\sqrt{2e/m_e}\frac{V^{3/2}}{d^2} \tag{4.16}$$

If we estimate the size of the last dynode as 1 square cm, and the distance from dynode to anode as 1 mm, and use the manufacter specified last dynode voltage $v = 122V$, then we have the maximum anode current $I_a = 130$ mA. For our PMT, the maximum current limit of $I_a = 90$ mA was found by increasing the incident light on it until the anode pulse was fully saturated.

4.2.5 Results

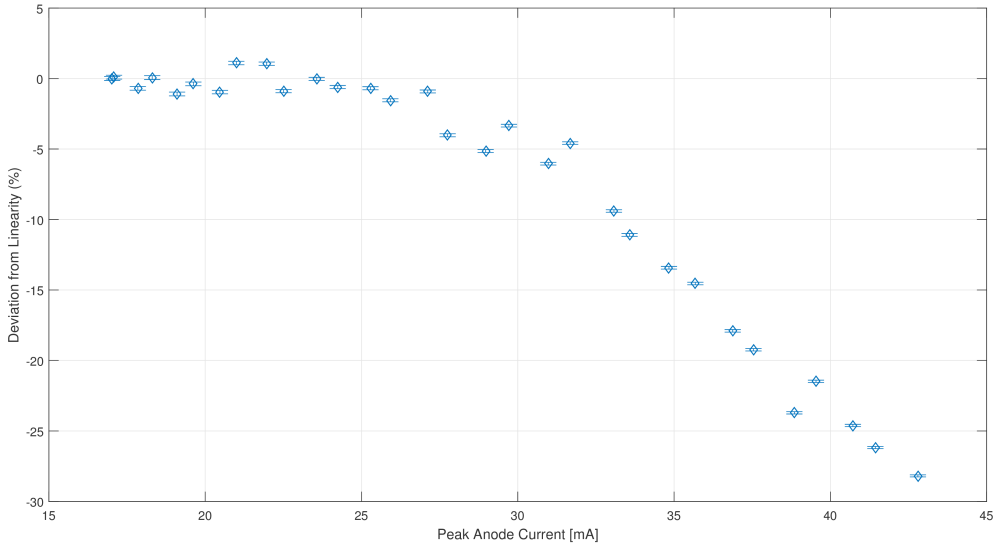

Figure 4.6: Pulsed charge nonlinearity of PMT KB0043 at -100°C. The general shape of a single pulse is shown in figure 3.5. Charge is calculated from the area of the digitized pulses. Frequency 1000 Hz, Pulse width 100 ns, Gain 1×10^7.

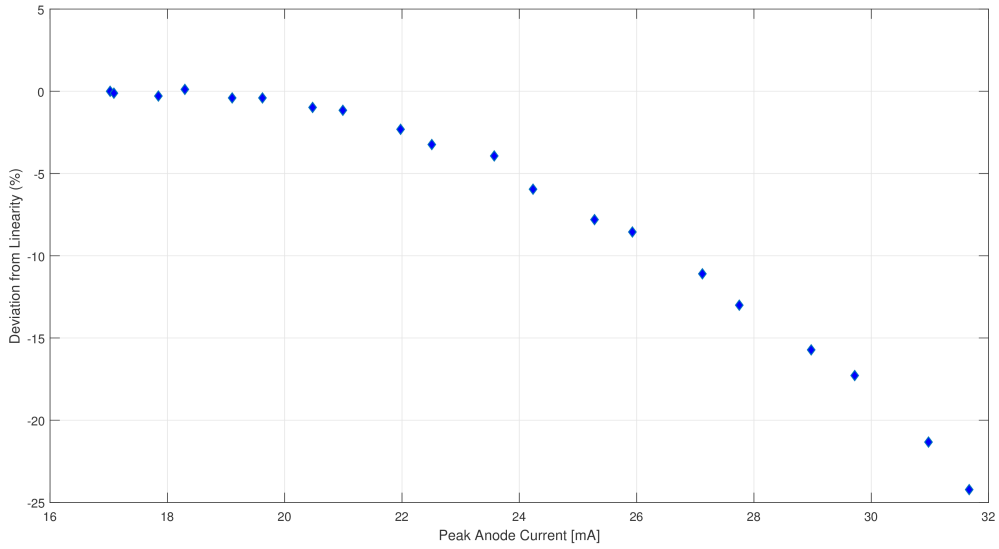

Figure 4.7: Pulsed current nonlinearity of PMT KB0043 at -100°C. The general shape of a single pulse is shown in figure 3.5. Current is calculated from the height of the digitized pulses. Frequency 1000 Hz, Pulse width 100 ns, Gain 1×10^7.

From the graphs shown above, it is clear that the decoupling capacitor values are sufficient for use in LZ, modeled by the 100 ns pulse width and 1 kHz frequency. There is no over-linearity as predicted by the voltage-divider circuit.

Our data is consistent with the manufacturer specification of 5% deviation at 20 mA peak anode current. At cryogenic temperatures, 5% current non-linearity is found to be 24 mA and charge non-linearity is 29 mA. This pulsed negative non-linearity is caused by space-charge effects, and not voltage redistribution from the voltage-divider circuit.

4.2.6 Future Work

The following experiments are proposed for future work in order to understand the nature of space charge saturation versus voltage divider effects:

1. While maintaining an input pulse of a specific size, increase the frequency of pulses in order to increase the mean anode current specifically. The deviation from linearity can be plotted as a function of pulse rate, the latter which is directly related to the mean anode current. In this way we can look for an positive non-linearity region as described in section . This will quantify the onset of mean anode current when the decoupling capacitors deplete themselves and can no longer prevent the voltage drop across the last dynode. If we do this for different sized pulses we can then compare the data with the prediction given by Eq. 4.12 in section 4.2.3.

2. Connect a separate HV supply to the last dynode stage, effectively creating a vacuum diode. Increase the voltage to plot the response of I_a, and compare to our graph of I_a as a function of number of photoelectrons, to see how anode current changes due to space charge.

Bibliography

[1] Young, BL. Front. Phys. (2017) 12: 121201. https://doi.org/10.1007/s11467-016-0583-4

[2] A Coc 2016 J. Phys.: Conf. Ser. 665 012001

[3] arXiv:1404.1938 - The Local Dark Matter Density

[4] arXiv:1507.03800 [hep-ph] - Indirect and direct search for dark matter

[5] arXiv:1511.00260 [physics.ins-det] - The dynamic range of LZ

[6] arXiv:1703.09144 [physics.ins-det] - LUX-ZEPLIN (LZ) Technical Design Report

[7] Photomultiplier tubes: principles and applications, Flyckt, Marmonier, 2002

[8] Photomultiplier tubes: basics and applications, 3rd Ed., Hamamatsu Photonics

[9] PA. T. Young, Photomultipliers: Their cause and cure, in Methods of Experimental Physics, N. Carleton, Ed. New York: Academic Press,1974, vol. 12, Astrophysics, Part A: Optical and Infrared

[10] arXiv:1108.3096 - An LED pulsar for measuring photomultiplier linearity

[11] ETEL Understanding Photomultipliers booklet

[12] AraÃžjo, H. & Chan, S. & Bugaev, V. & Blakemore C. (2016). LZ Photomultiplier Voltage-Divider Bases Circuit Design and Linearity Study. Unpublished manuscript for the LZ collaboration.

[13] D. J. Griffiths, Introduction to Electrodynamics, 3rd ed. (PrenticeHall, Englewood Cliffs, N.J., 1999), Chap. 2, pp. 107

[14] Nucl. Instr. and Meth.in Phys. Res. A, Land, P. L., 1971. A Discussion of the Region of Linear Operation of Photomultipliers.

[15] Discussion with Runxuan Liu (Brown University, LZ collaboration)

[16] arXiv:1802.06039 [astro-ph.IM] - Projected WIMP sensitivity of the LUX-ZEPLIN dark matter experiment